Nano Res. 2011, 4(1): 83–91
DOI 10.1007/s12274-010-0051-3
Research Article

ISSN 1998-0124
CN 11-5974/O4

# Synthesis of Pd Nanocrystals Enclosed by {100} Facets and with Sizes <10 nm for Application in CO Oxidation

Mingshang Jin[1,3,§], Hongyang Liu[2,§], Hui Zhang[1], Zhaoxiong Xie[3], Jingyue Liu[2,4], and Younan Xia[1] (✉)

[1] Department of Biomedical Engineering, Washington University, St. Louis, Missouri 63130, USA
[2] Center for Nanoscience, University of Missouri, St. Louis, Missouri 63121, USA
[3] State Key Laboratory for Physical Chemistry of Solid Surfaces, Department of Chemistry, Xiamen University, Xiamen, Fujian 361005, China
[4] Department of Physics and Astronomy, and Department of Chemistry and Biochemistry, University of Missouri, St. Louis, Missouri 63121, USA

Received: 23 August 2010 / Revised: 20 September 2010 / Accepted: 21 September 2010


## ABSTRACT

The catalytic activity of noble-metal nanocrystals is mainly determined by their sizes and the facets exposed on the surface. For single crystals, it has been demonstrated that the Pd(100) surface is catalytically more active than both Pd(110) and Pd(111) surfaces for the CO oxidation reaction. Here we report the synthesis of Pd nanocrystals enclosed by {100} facets with controllable sizes in the range of 6–18 nm by manipulating the rate of reduction of the precursor. UV–vis spectroscopy studies indicate that the rate of reduction of $Na_2PdCl_4$ can be controlled by adjusting the concentrations of $Br^-$ and $Cl^-$ ions added to the reaction mixture. Pd nanocrystals with different sizes were immobilized on ZnO nanowires and evaluated as catalysts for CO oxidation. We found that the activity of this catalytic system for CO oxidation showed a strong dependence on the nanocrystal size. When the size of the Pd nanocrystals was reduced from 18 nm to 6 nm, the maximum conversion rate was significantly enhanced by a factor of ~10 and the corresponding maximum conversion temperature was lowered by ~80 ˚C.

## KEYWORDS

Palladium, nanocubes, CO oxidation, size-dependence

Palladium (Pd) is a well-known and widely used heterogeneous and homogeneous catalyst with many industrial applications. It can catalyze a large number of reactions, including alkene hydrogenation [1–5], alcohol oxidation [6, 7], trichloroethene hydrodechlorination [8], as well as Suzuki [9, 10], Heck [11], and Stille coupling reactions [12]. Moreover, it can serve as a primary catalyst for the low-temperature reduction of automobile pollutants [13], petroleum cracking [14], CO oxidation [15–18], and electro-oxidation of formic acid [19–21]. All of these applications rely on the use of Pd nanoparticles or clusters well dispersed on a catalytic support or in a solution.

Over the past decade, ways of controlling the size and shape of Pd nanocrystals have attracted much attention because these two parameters allow one to

§ These two authors contributed equally to this work.
Address correspondence to xia@biomed.wustl.edu

tailor their intrinsic properties and thereby enhance their performance in various applications. For example, the conversion efficiency and selectivity of alkynes to alkenes, conjugated alkenes to monoalkenes, and hydrogenation of alkenes are all strongly dependent on the size of Pd nanocrystals [22–26], in particular, in the sub-10 nm regime. On the other hand, it has been demonstrated that the facets on the surface of Pd nanocrystals can have a strong influence on catalytic properties. So far, a wide variety of Pd nanocrystals with different shapes including cubes, bars, octahedra, plates, icosahedra, and pentagonal rods have all been prepared by carefully controlling reaction conditions such as temperature, reductants, capping agents, and concentrations of reagents and ionic species [27–38]. Nanoscale cubes and bars of Pd enclosed by {100} facets have received particular attention because these facets have been demonstrated to have a higher catalytic activity than {111} facets in some important reactions such as CO oxidation [39–45]. To this end, we and other groups have developed a simple strategy for the large-scale synthesis of Pd cubes and bars with sharp corners by introducing $Br^-$ as a capping agent and by taking advantage of its selective adsorption on {100} facets [27, 28]. Despite the early success, it still remains a great challenge to control the size of the Pd cubes and bars, particularly at scales below 10 nm.

Herein we describe a facile, aqueous approach for controlling the sizes of Pd cubes/bars in the range of 6–18 nm by adjusting the rate of reduction of $Pd^{2+}$ ions. The synthesis is based on a water-based process that involves injection of $Na_2PdCl_4$ into an aqueous solution of ascorbic acid (AA) held at 80 °C, with $Br^-$ ions serving as a capping agent and poly(vinyl pyrrolidone) (PVP) acting as a stabilizer. Control over the size of the Pd cubes/bars was achieved by introducing different amounts of halide species such as $Br^-$ and $Cl^-$. Besides capping the {100} facets of Pd nanocrystals, the halide species can also serve as coordination ligands to promote the formation of complexes such as $[PdBr_4]^{2-}$ and $[PdCl_4]^{2-}$ with $Pd^{2+}$ ions in aqueous solution, and thus reduce the rate of reduction of the $Pd^{2+}$ ions. Since the stability constant of $[PdBr_4]^{2-}$ is nearly $10^4$ times higher than that of $[PdCl_4]^{2-}$, it is clear that $Br^-$ binds $Pd^{2+}$ more strongly than $Cl^-$ [46, 47]. Therefore, introducing halide species such as $Br^-$ and $Cl^-$ not only results in the formation of Pd cubes/bars due to their selective capping of the {100} facets, but also greatly reduces the rate of reduction of $Pd^{2+}$ and thus the number of seeds formed in the initial stage. When the amount of the precursor is kept the same, the number of seeds and the size of the final product will be inversely proportional to each other.

In order to clarify the role of $Br^-$ in controlling the size of Pd nanocrystals, we conducted a set of experiments with different amounts of $Br^-$ being introduced. Figure 1(a) shows a typical transmission electron microscopy (TEM) image of the product obtained when 300 mg of KBr was added. The cubes/bars were 5 to 14 nm in size as measured by the width. The size distribution derived from the TEM image by counting ca. 150–200 cubes/bars is also plotted in Fig. 1(b). From this plot, the mean size of the Pd cubes/bars was found to be ~10 nm (width = 9.5 nm ± 4.5 nm, average aspect ratio = 1.2). When the amount of KBr was increased to 600 mg, we obtained Pd cubes/bars of ~18 nm (width = 18.0 nm ± 4.3 nm, average aspect ratio = 1.2) in size, as shown in Figs. 1(c) and 1(d). It is worth pointing out that the formation of Pd cubes/bars was also accompanied by a color change from reddish brown to black. The reaction rate can be estimated from the color change. In the case of 300 mg of KBr, the color change was observed at $t$ = 2 min. Further increasing the amount of KBr retarded the color change. With the addition of 600 mg KBr, the color of the solution remained unchanged for 5 min. It is clear that Pd cubes/bars with different sizes can be obtained by simply varying the amount of KBr introduced into the reaction system. As two additional examples, Pd cubes/bars of ~13 nm (width = 12.6 nm ± 4.3 nm, average aspect ratio = 1.2) and ~15 nm (width = 15.4 nm ± 3.7 nm, average aspect ratio = 1.2) in size were produced when 400 mg and 500 mg of KBr were introduced, respectively (Fig. S-1 in the Electronic Supplementary Material (ESM)).

In general, nanocrystal growth can be separated into two stages: nucleation and growth. The rate of reduction is one of the most important parameters in controlling the nucleation events. When the rate of reduction is high, more seeds will be formed in the nucleation stage. Obviously, more seeds will lead to

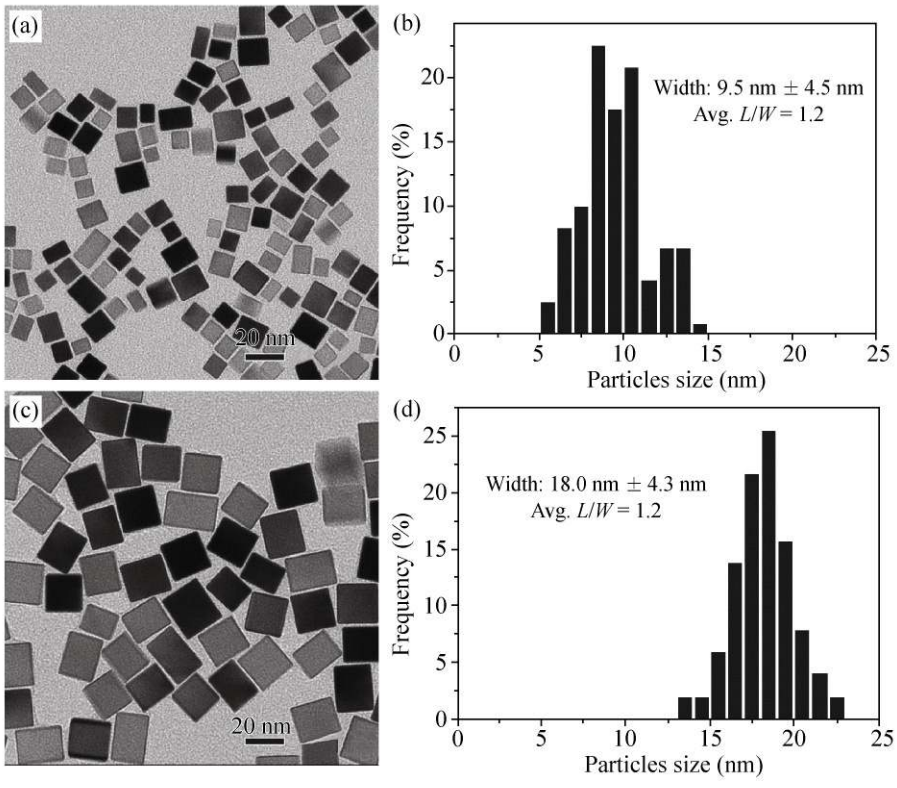


**Figure 1** TEM images of samples prepared in aqueous solutions containing 57 mg of $Na_2PdCl_4$, 105 mg of PVP, 60 mg of ascorbic acid, and (a) 300 mg of KBr and (c) 600 mg of KBr, and (b, d) the corresponding histograms of particle size distribution. For the cubes/bars, both width and average aspect ratio are used to describe their sizes

the formation of nanocrystals with smaller sizes when the amount of the precursor is kept the same. In this case, reducing the amount of KBr speeded up the rate of reduction of the precursor, and hence reduced the size of the Pd cubes/bars. As a result, one should be able to obtain Pd cubes/bars with smaller sizes (e.g., sub-10 nm) by further reducing the amount of KBr added. When only 5 mg KBr was introduced into the solution, the color changed very quickly, and Pd nanocrystals with a size of ~4 nm were obtained. Unfortunately, the cubic shape of the Pd nanocrystals was not maintained, as shown in Fig. S-2 (in the ESM). The product was dominated by irregularly shaped nanocrystals and a very small amount of cubes/bars, because there were not enough shape-directing ions (i.e., $Br^-$ ions) to cap the {100} facets. To overcome this problem, we introduced $Cl^-$ ions into the reaction mixture because $Cl^-$ can also act as a capping agent for Pd nanocrystals while showing weaker coordination ability for $Pd^{2+}$. In the synthesis of sub-10 nm Pd cubes/bars, the total molar concentration of halide ions was maintained the same as that with 300 mg of KBr, while different ratios of $Br^-/Cl^-$ were employed. Figure 2(a) shows a TEM image of the product obtained with the addition of 5 mg of KBr and 185 mg of KCl. In this case, we obtained sub-10 nm Pd cubes/ bars with sharp corners. From the corresponding size distribution histogram (Fig. 2(b)), the average size of the Pd cubes/bars was reduced to ~6 nm (width = 5.8 nm ± 2.2 nm, average aspect ratio = 1.4). The color of the solution started to change at $t$ = 30 s, indicating that the reduction in this case was much faster than the synthesis in which 300 mg KBr was introduced. When the $Br^-/Cl^-$ ratio was slightly increased (75 mg of KBr and 141 mg of KCl), the size of the resulting Pd cubes/ bars increased, as shown in Fig. 2(c). According to the size distribution histogram (Fig. 2(d)), the average size of the Pd cubes/bars was 7 nm (width = 7.3 nm ± 2.8 nm, average aspect ratio = 1.3). This work represents the first synthesis of sub-10 nm Pd cubes/bars, and this

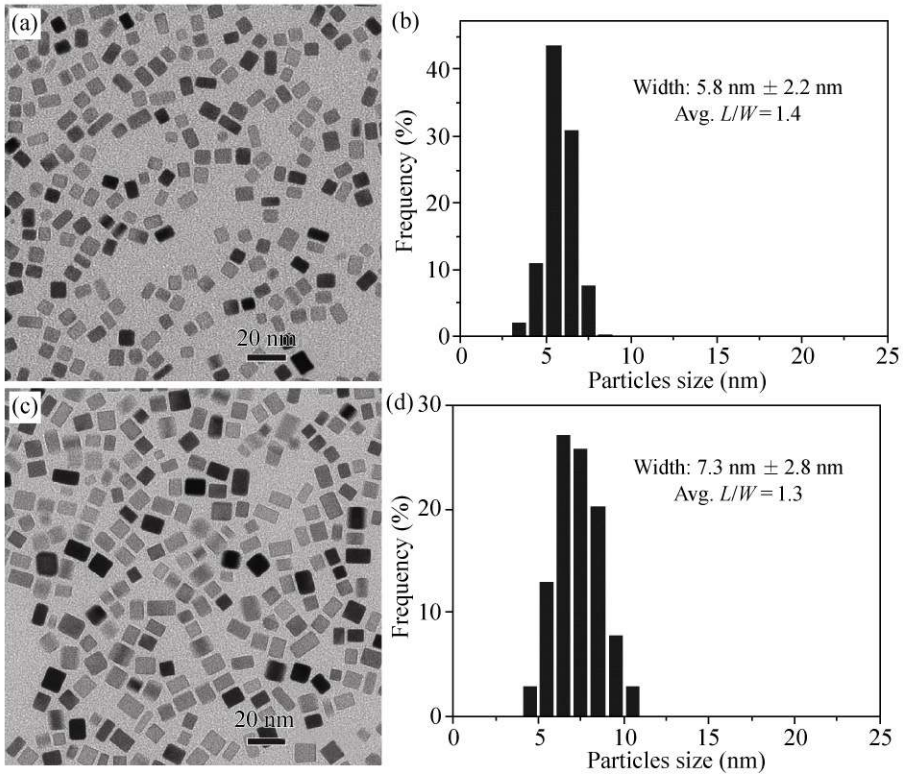


**Figure 2** TEM images of samples prepared in aqueous solutions containing 57 mg of $Na_2PdCl_4$, 105 mg of PVP, 60 mg of ascorbic acid, and different amounts of KCl and KBr: (a) 5 mg of KBr and 185 mg of KCl, and (c) 75 mg of KBr and141 mg of KCl. (b, d) The corresponding histograms of particle size distribution. The mixtures of halide salts contain the same total number of moles as that of 300 mg of KBr

approach may allow us to reduce the Pd cubes/bars down to even smaller sizes (e.g., 2 nm).

Based on the above observations, it can be concluded that the size of Pd cubes/bars can be easily controlled by varying the rate of reduction of $Pd^{2+}$ ions. To better account for the rates of reduction of $Pd^{2+}$ ions, UV–vis spectroscopy was employed to monitor the absorbance of the solution at different stages of the reactions for the syntheses of 6-, 10-, and 18-nm cubes/bars. As shown in Figs. 3(a)–3(c), there was an adsorption peak at ~245 nm, which can be attributed to $[PdCl_xBr_{4-x}]^{2-}$ [48, 49]. The concentration of the Pd precursor can be followed by plotting the change in absorbance at ~245 nm as a function of time (Fig. 3(d)). For the synthesis of 6-nm Pd cubes/bars, the consumption of the Pd precursor was much faster than in the syntheses of larger Pd nanocrystals, confirming that formation of smaller Pd cubes/bars results from a faster reduction rate, and vice versa. This result is also consistent with the observations of color changes. We can conclude that the number of seeds formed in the nucleation step can be experimentally controlled by introducing different amounts of halide ions.

The Pd cubes/bars having different sizes were then immobilized onto ZnO nanowires and used for catalytic studies. It was found that the Pd nanocrystals with different sizes showed a similar, well-dispersed distribution on ZnO nanowires (Fig. S-3 in the ESM). The catalytic oxidation of CO was used as a model reaction to examine the catalytic properties of Pd cubes/bars with different sizes. This system is ideal for the study of size-dependent effects in Pd catalysts as the effect of facets can be excluded here. The catalytic test was performed in a fixed-bed reactor (reaction conditions: flow rate 60 mL/min; 100 mg of Pd/ZnO catalyst; 2 wt% of Pd; $1.01 \times 10^5$ Pa pressure, 1% CO, 20% $O_2$, and He balance). Before catalytic testing, all the catalysts were pretreated at 100 ˚C for 2 h under 10% $O_2$/He (60 mL/min) [50]. Figure 4 summarizes the dependence of the CO conversion rate on the reaction

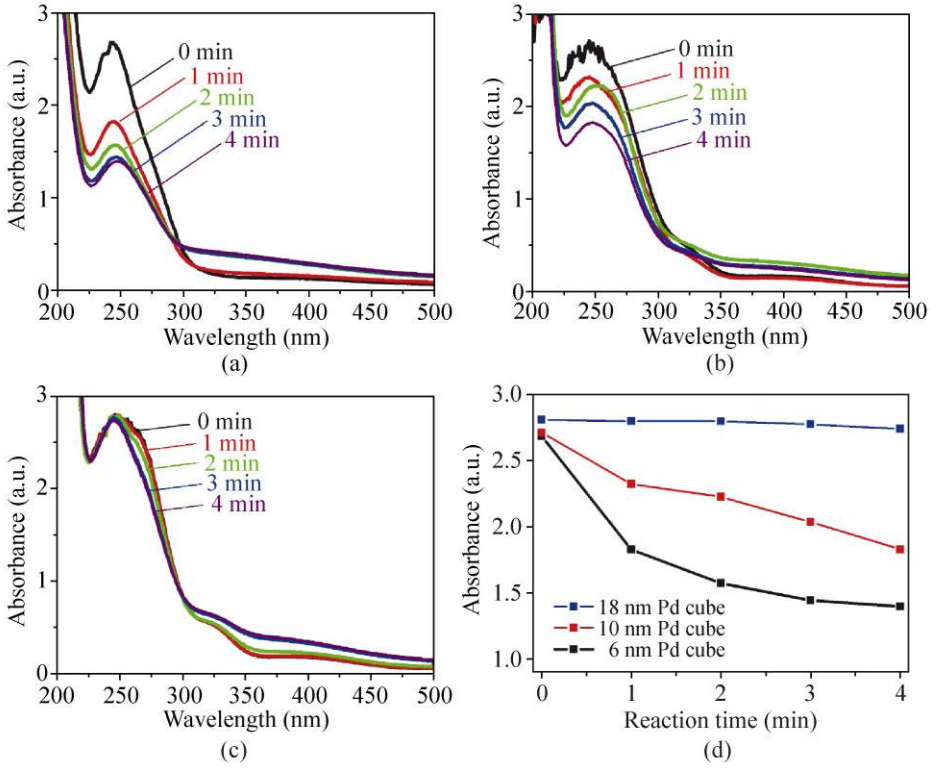


**Figure 3** UV–vis spectra of solutions taken at different reaction stages for the synthesis of: (a) 6-nm, (b) 10-nm, and (c) 18-nm Pd cubes/bars. (d) Time dependence of the absorbance at the peak position (~245 nm), which is directly proportional to the concentration of the $[PdCl_xBr_{4-x}]^{2-}$ species in the reaction solution

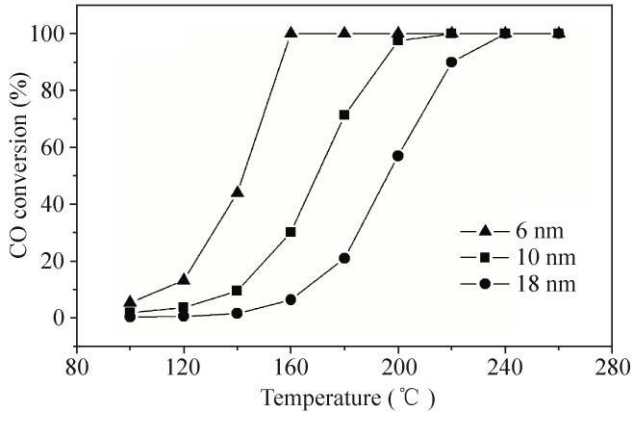


**Figure 4** CO conversion as a function of temperature for Pd cubes/bars with different sizes supported on ZnO nanowires. Reaction conditions: Pd/ZnO catalyst (100 mg); weight loading of Pd (2%); pressure ($1.01 \times 10^5$ Pa); reaction gas (1% CO, 20% $O_2$, and He balance)

temperature. The CO conversion over the 6-nm Pd cubes/bars was much higher than that over the 10- and 18-nm Pd cubes/bars. Decreasing the size of the Pd cubes/bars enhanced the conversion rate dramatically. The maximum conversion temperature also depends strongly on the sizes of the Pd cubes/bars. For example, for the 6-nm Pd cubes/bars, the maximum conversion temperature was 160 ℃, much lower than those for larger Pd nanocrystals. The intrinsic turnover frequency (TOF, defined here as CO conversion per surface Pd atom per second) was also dependent on the size of the Pd cubes/bars (Fig. 5). At a reaction temperature of 140 ℃, the TOF of the 6-nm Pd cubes/bars was approximately 3 and 10 times higher, respectively, than those of the 10- and 18-nm Pd cubes/bars. Since the TOF reflects the intrinsic activity of the surface sites, Fig. 5 clearly demonstrates that the size of the Pd cubes/bars strongly influences the nature of the catalytically active sites on the nanocrystals, which is consistent with the previous studies of CO oxidation on a Pd/MgO (100) model catalyst [51]. The dependence of CO oxidation on particle size can also be possibly attributed to other factors, including structural effects,

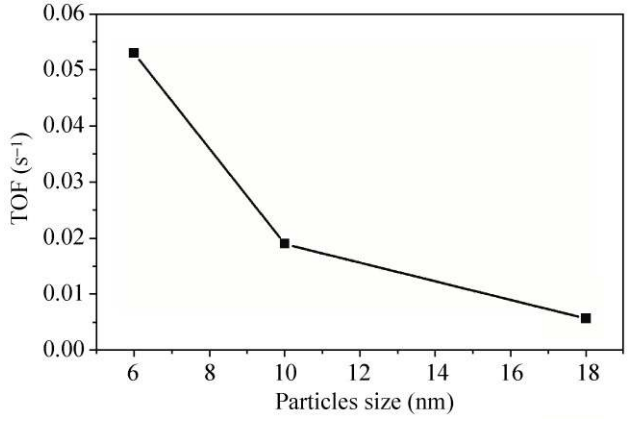


**Figure 5** Turnover frequencies (TOFs) of CO conversion at 140 ˚C over ZnO-supported Pd cubes/bars with different sizes. The TOF was calculated on the basis of CO molecule per surface Pd atom. Reaction conditions: Pd/ZnO catalyst (100 mg); weight loading of Pd (2%); pressure ($1.01 \times 10^5$ Pa); reaction gas (1% CO, 20% $O_2$, and He balance)

electronic effects, metal-support interaction, and formation of an active surface oxide layer. Although we need to further investigate the origin of the size-dependent TOF of the Pd cubes/bars for CO oxidation, our results showed unambiguously, for the first time, that the size of the shape-controlled Pd cubes/bars determines their TOF for catalytic CO oxidation reaction.

In summary, we have succeeded in preparing sub-10 nm Pd cubes/bars by controlling the rate of reduction. Using this kinetic approach, the sizes of Pd nanocrystals can be tuned in the range of 6 to 18 nm. We then immobilized the Pd cubes/bars with different sizes onto ZnO nanowires and evaluated their catalytic performance in the CO oxidation reaction. Compared with the 18-nm Pd cubes/bars, the maximum conversion temperature for CO oxidation was 80 ˚C lower and the TOF was about 10 times higher for the 6-nm Pd cubes/bars, suggesting that smaller Pd cubes/bars may be better for low temperature CO oxidation reactions. Our results clearly show that the size of the Pd cubes/bars enclosed by {100} facets determines the TOF for CO oxidation reactions.

## Experimental

**Synthesis of Pd cubes/bars.** In a typical synthesis of Pd cubes/bars with different sizes, 8.0 mL of an aqueous solution containing poly(vinyl pyrrolidone) (PVP, $M_W \approx 55\,000$, 105 mg, Aldrich), *L*-ascorbic acid (AA, 60 mg, Aldrich), and different amounts of KBr and KCl were placed in a 20 mL vial, and pre-heated in air under magnetic stirring at 80 ˚C for 10 min. Then, 3.0 mL of an aqueous solution containing $Na_2PdCl_4$ (57 mg, Aldrich) was added using a pipette. After the vial had been capped, the reaction was allowed to proceed at 80 ˚C for 3 h. The product was collected by centrifugation and washed 10 times with water to remove excess PVP.

**Synthesis of the ZnO nanowire support.** We followed the protocol developed by Wang and co-workers for the preparation of ZnO nanowires [52]. In a typical procedure, a mixture of ZnO and carbon powder was placed in a ceramic boat inside a tube furnace, and a Si substrate was placed downstream to collect the ZnO nanowires. The horizontal distance between the source and the substrate was about 2–3 cm. Prior to heating, the quartz tube was purged with Ar gas (99.9%) for 30 min. The tube furnace was heated to 1000 ˚C for 60 min. After cooling the tube furnace to room temperature, ZnO nanowires were collected from the Si substrate.

**Preparation of Pd on ZnO catalysts.** The preparation of each Pd/ZnO catalyst involved three steps: (1) the ZnO nanowires were dispersed in ethanol by sonication; (2) the as-prepared Pd nanocrystals were added into the solution with vigorous magnetic stirring; and (3) the Pd/ZnO catalyst was collected by filtration, washed with ethanol, and kept in an oven overnight at 100 ˚C.

**Evaluation of catalytic activity.** The activities of the Pd/ZnO catalysts for CO oxidation were evaluated in a home-made, fixed-bed quartz tubular reactor [53]. The Pd/ZnO catalysts (100 mg, 2 wt% of Pd) were placed in the reactor. The reactant gases (1.0% CO, 20% $O_2$, and He balance) were passed through the reactor at a rate of 60 mL/min. The composition of the reaction products exiting the reactor was monitored by a gas chromatography.

**Characterization.** For TEM, the nanocrystals were dispersed in ethanol and then dropped on carbon-coated copper grids. TEM images were obtained using

a Philips 420 transmission electron microscope operated at 120 kV. The concentrations of the catalyst samples were determined using inductively coupled plasma mass spectrometry (ICP-MS) (PerkinElmer Elan DRC Ⅱ ICP-MS) measurements. For UV–vis characterization, 25 μL of reaction solution was diluted with 3 mL 18 MΩ water, and spectra recorded with a Cary 50 spectrometer (Varian).

## Acknowledgements

This work was supported in part by the NSF (DMR-0804088) and startup funds from Washington University in St. Louis. As a visiting student from Xiamen University, M. J. was also partially supported by the China Scholarship Council (CSC). Part of the work was performed at the Nano Research Facility (NRF), a member of the National Nanotechnology Infrastructure Network (NNIN), which is supported by the NSF under award no. ECS-0335765. H. L. and J. L. were supported by the University of Missouri-St. Louis.

**Electronic Supplementary Material:** Supplementary material is available in the online version of this article at http://dx.doi.org/10.1007/s12274-010-0051-3 and is accessible free of charge.



## References

[1] Doyle, A. M.; Shaikhutdinov, S. K.; Freund, H. J.; Freund, J. Surface-bonded precursor determines particle size effects for alkene hydrogenation on palladium. *Angew. Chem. Int. Edit.* **2005**, *44*, 629–631.

[2] Doyle, A. M.; Shaikhutdinov, S. K.; Jackson, S. D.; Freund, H. J. Hydrogenation on metal surfaces: Why are nanoparticles more active than single crystals? *Angew. Chem. Int. Edit.* **2003**, *42*, 5240–5243.

[3] Shaikhutdinov, S. K.; Heemeier, M.; Baumer, M.; Lear, T.; Lennon, D.; Oldman, R. J.; Jackson, S. D.; Freund, H. J. Structure-reactivity relationships on supported metal model catalysts: Adsorption and reaction of ethene and hydrogen on $Pd/Al_2O_3/NiAl(110)$. *J. Catal.* **2001**, *220*, 330–339.

[4] Wilson, O. M.; Knecht, M. R.; Garcia-Martinez, J. C.; Crooks, R. M. Effect of Pd nanoparticle size on the catalytic hydrogenation of allyl alcohol. *J. Am. Chem. Soc.* **2006**, *128*, 4510–4511.

[5] Bhattacharjee, S.; Dotzauer, D. M.; Bruening, M. L. Selectivity as a function of nanoparticle size in the catalytic hydrogenation of unsaturated alcohols. *J. Am. Chem. Soc.* **2009**, *131*, 3601–3610.

[6] Chen, J.; Zhang, Q. H.; Wang, Y.; Wan, H. L. Size-dependent catalytic activity of supported palladium nanoparticles for aerobic oxidation of alcohols. *Adv. Synth. Catal.* **2008**, *350*, 453–464.

[7] Li, F.; Zhang, Q. H.; Wang, Y. Size dependence in solvent-free aerobic oxidation of alcohols catalyzed by zeolite-supported palladium nanoparticles. *Appl. Catal. A* **2008**, *334*, 217–226.

[8] He, F.; Liu, J. C.; Roberts, C. B.; Zhao, D. Y. One-step "green" synthesis of Pd nanoparticles of controlled size and their catalytic activity for trichloroethene hydrodechlorination. *Ind. Eng. Chem. Res.* **2009**, *48*, 6550–6557.

[9] Li, Y.; Boone, E.; El-Sayed, M. A. Size effects of PVP–Pd nanoparticles on the catalytic Suzuki reactions in aqueous solution. *Langmuir* **2002**, *18*, 4921–4925.

[10] Narayanan, R.; El-Sayed, M. A. Effect of colloidal catalysis on the nanoparticle size distribution: Dendrimer–Pd vs. PVP–Pd nanoparticles catalyzing the Suzuki coupling reaction. *J. Phys. Chem. B* **2004**, *108*, 8572–8580.

[11] Le Bars, J.; Specht, U.; Bradley, J. S.; Blackmond, D. G. A catalytic probe of the surface of colloidal palladium particles using Heck coupling reactions. *Langmuir* **1999**, *15*, 7621–7625.

[12] Garcia-Martinez, J. C.; Lezutekong, R.; Crooks, R. M. Dendrimer-encapsulated Pd nanoparticles as aqueous, room-temperature catalysts for the Stille reaction. *J. Am. Chem. Soc.* **2005**, *127*, 5097–5103.

[13] Nishihata, Y.; Mizuki, J.; Akao, T.; Tanaka, H.; Uenishi, M.; Kimura, M.; Okamoto, T.; Hamada, N. Self-regeneration of a Pd-perovskite catalyst for automotive emissions control. *Nature* **2002**, *418*, 164–167.

[14] Thomas, J. M.; Johnson, B. F. G.; Raja, R.; Sankar, G.; Midgley, P. A. High-performance nanocatalysts for single-step hydrogenations. *Acc. Chem. Res.* **2003**, *36*, 20–30.

[15] Fernandez-Garcia, M.; Martinez-Arias, A.; Salamanca, L. N.; Coronado, J. M.; Anderson, J. A.; Conesa, J. C.; Soria, J. Influence of ceria on Pd activity for the $CO + O_2$ reaction. *J. Catal.* **1999**, *187*, 474–485.

[16] Coulston, G. W.; Haller, G. L. The dynamics of Co oxidation

on Pd, Rh, and Pt studied by high-resolution infrared chemiluminescence spectroscopy. *J. Chem. Phys.* **1991**, *95*, 6932–6944.

[17] Chen, M. S.; Cal, Y.; Yan, Z.; Gath, K. K.; Axnanda, S.; Goodman, D. W. Highly active surfaces for CO oxidation on Rh, Pd, and Pt. *Surf. Sci.* **2007**, *601*, 5326–5331.

[18] Nakao, K.; Watanabe, O.; Sasaki, T.; Ito, S.; Tomishige, K.; Kunimori, K. CO oxidation on Pd(111), Pt(111), and Rh(111) surfaces studied by infrared chemiluminescence spectroscopy. *Surf. Sci.* **2007**, *601*, 3796–3800.

[19] Huang, X. Q.; Tang, S. H.; Zhang, H. H.; Zhou, Z. Y.; Zheng, N. F. Controlled formation of concave tetrahedral/trigonal bipyramidal palladium nanocrystals. *J. Am. Chem. Soc.* **2009**, *131*, 13916–13917.

[20] Zhou, W. P.; Lewera, A.; Larsen, R.; Masel, R. I.; Bagus, P. S.; Wieckowski, A. Size effects in electronic and catalytic properties of unsupported palladium nanoparticles in electrooxidation of formic acid. *J. Phys. Chem. B* **2006**, *110*, 13393–13398.

[21] Zhou, W. J.; Lee, J. Y. Particle size effects in Pd-catalyzed electrooxidation of formic acid. *J. Phys. Chem. C* **2008**, *112*, 3789–3793.

[22] Semagina, N.; Renken, A.; Kiwi-Minsker, L. Palladium nanoparticle size effect in 1-hexyne selective hydrogenation. *J. Phys. Chem. C* **2007**, *111*, 13933–13937.

[23] Semagina, N.; Renken, A.; Laub, D.; Kiwi-Minsker, L. Synthesis of monodispersed palladium nanoparticles to study structure sensitivity of solvent-free selective hydrogenation of 2-methyl-3-butyn-2-ol. *J. Catal.* **2007**, *246*, 308–314.

[24] Tardy, B.; Noupa, C.; Leclercq, C.; Bertolini, J. C.; Hoareau, A.; Treilleux, M.; Faure, J. P.; Nihoul, G. Catalytic-hydrogenation of 1,3-butadiene on Pd particles evaporated on carbonaceous supports: Particle size effect. *J. Catal.* **1991**, *129*, 1–11.

[25] Silvestre-Albero, J.; Rupprechter, G.; Freund, H. J. Atmospheric pressure studies of selective 1,3-butadiene hydrogenation on well-defined $Pd/Al_2O_3/NiAl(110)$ model catalysts: Effect of Pd particle size. *J. Catal.* **2006**, *240*, 58–65.

[26] Vasylyev, M. V.; Maayan, G.; Hovav, Y.; Haimov, A.; Neumann, R. Palladium nanoparticles stabilized by alkylated polyethyleneimine as aqueous biphasic catalysts for the chemoselective stereocontrolled hydrogenation of alkenes. *Org. Lett.* **2006**, *8*, 5445–5448.

[27] Lim, B.; Jiang, M. J.; Tao, J.; Camargo, P. H. C.; Zhu, Y. M.; Xia, Y. N. Shape-controlled synthesis of Pd nanocrystals in aqueous solutions. *Adv. Funct. Mater.* **2009**, *19*, 189–200.

[28] Niu, W. X.; Li, Z. Y.; Shi, L. H.; Liu, X. Q.; Li, H. J.; Han, S.; Chen, J.; Xu, G. B. Seed-mediated growth of nearly monodisperse palladium nanocubes with controllable sizes. *Cryst. Growth Des.* **2008**, *8*, 4440–4444.

[29] Lim, B.; Kobayashi, H.; Camargo, P. H. C.; Allard, L. F.; Liu, J. Y.; Xia, Y. N. New insights into the growth mechanism and surface structure of palladium nanocrystals. *Nano Res.* **2010**, *3*, 180–188.

[30] Lim, B.; Xiong, Y. J.; Xia, Y. N. A water-based synthesis of octahedral, decahedral, and icosahedral Pd nanocrystals. *Angew. Chem. Int. Ed.* **2007**, *46*, 9279–9282.

[31] Xia, Y.; Xiong, Y. J.; Lim, B.; Skrabalak, S. E. Shape-controlled synthesis of metal nanocrystals: Simple chemistry meets complex physics? *Angew. Chem. Int. Ed.* **2009**, *48*, 60–103.

[32] Xiong, Y. J.; Cai, H. G.; Wiley, B. J.; Wang, J. G.; Kim, M. J.; Xia, Y. N. Synthesis and mechanistic study of palladium nanobars and nanorods. *J. Am. Chem. Soc.* **2007**, *129*, 3665–3675.

[33] Xiong, Y. J.; Cai, H. G.; Yin, Y. D.; Xia, Y. N. Synthesis and characterization of fivefold twinned nanorods and right bipyramids of palladium. *Chem. Phys. Lett.* **2007**, *440*, 273–278.

[34] Chen, Y. H.; Hung, H. H.; Huang, M. H. Seed-mediated synthesis of palladium nanorods and branched nanocrystals and their use as recyclable Suzuki coupling reaction catalysts. *J. Am. Chem. Soc.* **2009**, *131*, 9114–9121.

[35] Tian, N.; Zhou, Z. Y.; Sun, S. G. Electrochemical preparation of Pd nanorods with high-index facets. *Chem. Commun.* **2009**, 1502–1504.

[36] Yu, Y. C.; Zhao, Y. X.; Huang, T.; Liu, H. F. Microwave-assisted synthesis of palladium nanocubes and nanobars. *Mater. Res. Bull.* **2010**, *45*, 159–164.

[37] Chang, G.; Oyama, M.; Hirao, K. Facile synthesis of monodisperse palladium nanocubes and the characteristics of self-assembly. *Acta Mater.* **2007**, *55*, 3453–3456.

[38] Shen, X. S.; Wang, G. Z.; Hong, X.; Zhu, W. Simple-cubic microcubes assembled by palladium nanocubes. *CrystEngComm* **2009**, *11*, 753–755.

[39] Zhang, C. J.; Hu, P. CO oxidation on Pd(100) and Pd(111): A comparative study of reaction pathways and reactivity at low and medium coverages. *J. Am. Chem. Soc.* **2001**, *123*, 1166–1172.

[40] Nakao, K.; Ito, S.; Tomishige, K.; Kunimori, K. Structure of activated complex of $CO_2$ formation in a $CO + O_2$ reaction on Pd(110) and Pd(111). *J. Phys. Chem. B* **2005**, *109*, 17553–17559.

[41] Nakao, K.; Ito, S. I.; Tomishige, K.; Kunimori, K. Reaction mechanism and structure of activated complex of $CO_2$ formation in CO oxidation on Pd(110) and Pd(111) surfaces. *Catal. Today* **2006**, *111*, 316–321.

[42] Nakao, K.; Ito, S.; Tomishige, K.; Kunimori, K. Infrared chemiluminescence study of CO + $O_2$ reaction on Pd(110): Activated complex of $CO_2$ formation at high CO coverage. *Chem. Phys. Lett.* **2005**, *410*, 86–89.

[43] Nakao, K.; Ito, S.; Tomishige, K.; Kunimori, K. Infrared chemiluminescence study of $CO_2$ formation in CO plus NO reaction on Pd(110) and Pd(111) surfaces. *J. Phys. Chem. B* **2005**, *109*, 17579–17586.

[44] Uetsuka, H.; Watanabe, K.; Ohnuma, H.; Kunimori, K. Structure sensitivity of the dynamics of CO oxidation on Pd(111), Pd(110) and polycrystalline Pd surfaces: Infrared chemiluminescence study of the product $CO_2$. *Chem. Lett.* **1996**, *25*, 227–228.

[45] Uetsuka, H.; Watanabe, K.; Ohnuma, H.; Kunimori, K. Structure-sensitivity in the dynamics of CO oxidation over Pd surfaces: Infrared chemiluminescence of the product $CO_2$. *Surf. Rev. Lett.* **1997**, *4*, 1359–1363.

[46] Srivastava, S. C.; Newman, L. Mixed ligand complexes of palladium(Ⅱ) with chloride and bromide. *Inorg. Chem.* **1966**, *5*, 1506–1510.

[47] Feldberg, S.; Klotz, P.; Newman, L. Computer evaluation of equilibrium constants from spectrophotometric data. *Inorg. Chem.* **1972**, *11*, 2860–2865.

[48] Wang, Z. F.; Shen, B.; He, N. Y. The synthesis of Pd nanoparticles by combination of the stabilizer of $CNCH_2COOK$ with its reduction. *Mater. Lett.* **2004**, *58*, 3652–3655.

[49] Xiong, Y. J.; Chen, J. Y.; Wiley, B.; Xia, Y. N. Understanding the role of oxidative etching in the polyol synthesis of Pd nanoparticles with uniform shape and size. *J. Am. Chem. Soc.* **2005**, *127*, 7332–7333.

[50] Kuhn, J. N.; Tsung, C. K.; Huang, W.; Somorjai, G. A. Effect of organic capping layers over monodisperse platinum nanoparticles upon activity for ethylene hydrogenation and carbon monoxide oxidation. *J. Catal.* **2009**, *265*, 209–215.

[51] Becker, C.; Henry, C. R. Cluster size dependent kinetics for the oxidation of CO on a Pd/MgO(100) model catalyst. *Surf. Sci.* **1996**, *352*, 457–462.

[52] Pan, Z. W.; Dai, Z. R.; Wang, Z. L. Nanobelts of semiconducting oxides. *Science* **2001**, *291*, 1947–1949.

[53] Liu, H.Y.; Liu, J. Faceted ZnO nanowire supported Pd catalyst for the methanol steam reforming. *Microsc. Microanal.* **2010**, *16*, 1206–1207.